

# Three water sites in upper mantle olivine and the role of titanium in the water weakening mechanism

A. M. Walker,<sup>1</sup> J. Hermann,<sup>1</sup> A. J. Berry,<sup>2</sup> and H. St. C. O'Neill<sup>1</sup>

---

A. M. Walker, Department of Earth Sciences, University of Cambridge, Downing Street, Cambridge, CB2 3EQ, UK. (amw75@cam.ac.uk)

<sup>1</sup>Research School of Earth Sciences, The Australian National University, Mills Road, Canberra, ACT 0200, Australia

<sup>2</sup>Department of Earth Science and Engineering, Imperial College London, South Kensington, London, SW7 2AZ, United Kingdom

**Abstract.**

Infrared spectroscopy on synthetic olivines has established that there are at least four different mechanisms by which hydrogen is incorporated into the crystal structure. Two mechanisms occur in the system  $\text{MgO-SiO}_2\text{-H}_2\text{O}$  associated with silicon and magnesium vacancies respectively. A third mechanism is associated with trivalent cation substitution, commonly  $\text{Fe}^{3+}$  in natural olivine, while the fourth mechanism, which is the one most prevalent in natural olivines from the spinel-peridotite facies of the Earth's upper mantle, is associated with  $\text{Ti}^{4+}$  [Berry *et al.* 2005; *Geology* **33**(11) pp.869-872]. Here, first principles calculations based on density functional theory are used to derive the structure and relative energies of the two defects in the pure  $\text{MgO-SiO}_2\text{-H}_2\text{O}$  system, and possible hydrogen-bearing and hydrogen-free point defects in  $\text{Ti}^{4+}$ -doped forsterite. Calculated structures are used to compare the predicted orientation of the O-H bonds with the experimentally determined polarisation. The energies are used to discuss how different regimes of chemical environment, temperature (T), pressure (P), and both water content and water fugacity ( $f_{\text{H}_2\text{O}}$ ), impact on which of the different hydroxyl substitution mechanisms are thermodynamically stable. We find that given the presence of Ti impurities, the most stable mechanism involves the formation of silicon vacancies containing two protons charge balanced by a  $\text{Ti}^{4+}$  cation occupying an adjacent octahedral site. This mechanism leads to the water mediated formation of silicon vacancies. As silicon is known to be the

most slowly diffusing species in olivine this provides a credible explanation of the observed water weakening effect in olivine.

## 1. Introduction

The great affect of small amounts of hydrogen on the physical properties of the nominally anhydrous minerals (NAMs) that make up Earth's upper mantle is well known and has been the subject of extensive study. The substitution of hydrogen in silicate minerals occurs by bonding to lattice oxygen to form hydroxyl groups ( $\text{OH}^-$ ), and such hydroxyl is colloquially known in the petrologic literature as "water". In olivine, the important effects of hydrogen include a major decrease in strength in both the dislocation and diffusional creep regime [Mei and Kohlstedt, 2000a, b], an increase in electrical conductivity [Karato, 1990; Wang *et al.*, 2006; Yoshino *et al.*, 2006] and a postulated increase in the attenuation of seismic energy [Karato and Jung, 1998]. These changes have important implications for understanding the behaviour of our planet. For example, a plausible explanation for the dramatic difference in the global tectonic processes occurring on Venus and Earth [Solomon *et al.*, 1991] is the presence of low concentrations of water dissolved in the terrestrial mantle, decreasing the upper mantle viscosity on Earth when compared to Venus [Kaula, 1990, 1995] and permitting the development of subduction zones on Earth [Regenauer-Lieb *et al.*, 2001; Regenauer-Lieb and Kohl, 2003]. It is also possible that diffusing hydrogen ions are the main charge carriers in the mantle, dominating the observed electromagnetic response. For example, Lizarralde *et al.* [1995] and Evans *et al.* [1999] suggest that hydrogen diffusion through olivine is active under the Pacific while a recent analysis suggests that this could be the main mechanism of electrical conductivity active in the anisotropic sub-continental upper mantle in a study area under northern Europe [Gatzemeier and Moorkamp, 2005].

In order to understand how dissolved water so drastically affects physical properties, it is first necessary to determine the mechanisms leading to its incorporation in NAMs. A powerful tool to probe the local structure around the  $\text{OH}^-$  groups in NAMs is infrared (IR) spectroscopy. For pure synthetic forsterite in the simple system  $\text{MgO-SiO}_2\text{-H}_2\text{O}$ , experiments where the silica activity was varied yield distinct IR fingerprints that clearly distinguish when forsterite is buffered by MgO (IR absorbance peaks close to 3612, 3579 and  $3567\text{ cm}^{-1}$ , see Figure 1) from when forsterite is buffered by pyroxene (broad peaks at 3160 and  $3220\text{ cm}^{-1}$ ). The interpretation of this result is that hydrated silicon vacancies (that is, a vacant silicon site with each of the four oxygen atoms surrounding the vacancy bonded to hydrogen atoms) form when the system is MgO-buffered and hydrated magnesium vacancies (a magnesium vacancy with two of the surrounding oxygen atoms bonded to hydrogen atoms) form in the pyroxene-buffered case [Matveev *et al.*, 2001; Lemaire *et al.*, 2004]. This interpretation posed a problem for the understanding of the spectra of natural mantle-derived samples, as their most common IR fingerprint from the spinel-peridotite facies (peaks close to 3572 and  $3525\text{ cm}^{-1}$ ) is more similar to that found in the MgO-buffered experiments, despite the presence of pyroxene in the Earth's upper mantle [Matveev *et al.*, 2001]. The explanation for this seeming paradox is that the spectra of the natural olivines is actually due to a third type of substitution, in which the  $\text{OH}^-$  group is associated with Ti, a trace element substituting in natural olivines [Berry *et al.*, 2005]. This titanium fingerprint is present whether the sample is buffered by MgO or pyroxene and is similar to the group I peaks of Bai and Kohlstedt [1993]. To complicate matters still further, a fourth type of defect associated with trivalent cation impurities has been identified [Berry *et al.* in prep], which produces peaks in the IR spectra at 3355 and

3325  $\text{cm}^{-1}$  in Fe-bearing olivines associated with  $\text{Fe}^{3+}$ , perhaps produced by late-stage oxidation [Berry *et al.*, 2005]. In addition to these common fingerprints, exotic samples collected from atypical localities can host much more hydrogen and display many more peaks in the IR spectra. For example, Koch-Müller *et al.* [2006] and Matsyuk and Langer [2004] describe suites of “wet” xenocrysts from kimberlite pipes and other mantle derived olivines and identify 23 and 70 IR peaks respectively. We do not consider these complex and unusual spectra here and concentrate on the simple spectra observed from experiment and typically “dry” olivine samples, such as those from olivine xenocrysts from San Carlos, Arizona studied by Berry *et al.* [2005] and reported in Figure 1.

The recognition that hydrogen is incorporated in olivine by several different mechanisms raises the question of which mechanisms are stable under which conditions. To investigate this, we have undertaken first principles calculations based on density functional theory to derive the structure and relative energies of the two defects in the pure  $\text{MgO-SiO}_2$  system, and possible hydrogen-bearing and hydrogen-free point defects in  $\text{Ti}^{4+}$ -doped forsterite. The temperature and pressure dependence of these three defect types is also calculated, allowing a quantitative assessment of their relative stabilities as a function of these variables as well as chemical environment including water content and fugacity ( $f_{\text{H}_2\text{O}}$ ).

## 2. Methodology

First principles calculations aim to simulate the behaviour of matter at the atomic scale without relying on experimental information, apart from some fundamental physical constants. The key step is to calculate the ground state energy of a system consisting of electrons in an external potential field describing the interactions between the elec-

trons and atomic nuclei; this requires the solution of the (time independent) Schrödinger equation. For condensed matter, the dominant approach is to transform the Schrödinger equation into a form where the energy of the system is written as a functional of the electron density. This procedure leads to a mathematically exact expression for the energy and avoids the need for the calculation of the many body wavefunction. The cost of this procedure is the need to introduce an approximate exchange - correlation functional (the existence of an exact exchange - correlation functional can be proven, however, its form is both complex and unknown). With the ability to calculate the energy of any arrangement of nuclei, one can move nuclei around in order to find energy minima which correspond to stable or metastable structures. In the present application these structures correspond to defects in forsterite crystals. The model of the defects makes use of periodic boundary conditions to remove boundary effects and a three-stage process is used in order to identify the role of titanium on the incorporation of water in forsterite. The mechanism of titanium incorporation in hydrogen free forsterite is examined by calculating the energies and structures of various simulation cells containing titanium(IV) and other charge compensating defects, if they are required. The incorporation mechanism of hydrogen in titanium free forsterite is examined by calculating the energies and structures of cells with cation vacancies surrounded by charge compensating hydrogen ions, which are bonded to the oxygen atoms around the vacant polyhedra. Finally, possible reactions between the point defects that form during the process of titanium and hydrogen incorporation are considered by calculating the structure and energies of cells containing composite defects and comparing the energies with the unbound but charge neutral alternatives.

## 2.1. Computational details

In order to calculate the energies of the various possible hydrogen and titanium incorporation mechanisms, and to establish the structure of the resulting defects, we modelled a wide range of point defects in forsterite. The point defects studied were all charge neutral and included those that may form as a result of titanium incorporation in dry forsterite, silicon and magnesium vacancies surrounded by hydroxyl groups and various possible defect clusters containing both titanium and hydrogen associated with cation vacancies. Each of the defects was embedded in a  $2 \times 1 \times 2$  forsterite supercell. This gives a unit cell in which the smallest dimension is approximately 9.6 Å, sufficiently large to minimise undesirable defect - defect interactions, allowing the energies to be considered as those for a dilute population of defects [Richmond and Brodholt, 2000].

Density Functional Theory [Hohenberg and Kohn, 1964; Kohn and Sham, 1965] as implemented using the SIESTA methodology [Soler *et al.*, 2002] was used to calculate the energies and find the minimum energy configuration of all the simulation cells. Calculations were performed within the Generalized Gradient Approximation using the exchange - correlation functional of Perdew *et al.* [1996]. The SIESTA methodology makes use of a numerical basis of a linear combination of pseudo-atomic orbitals to describe the valence electrons, and pseudopotentials to describe the core electrons and nuclei. This approach allows the large number of possible defect configurations to be studied without unfeasible computational requirements. For all atom types, the valence orbitals were described using a double-zeta polarized basis consisting of atomic orbitals that were confined within a smooth potential that becomes asymptotic to infinity at a chosen radius [Junquera *et al.*, 2001]. Within the SIESTA methodology, an auxiliary basis set is employed to compute



the exchange-correlation and Hartree energies, consisting of a uniform real space grid. A kinetic energy cut-off of 250 Ry and  $2\times 2\times 2$  grid cell sampling was used in order to yield sufficient numerical convergence.

In addition to performing calculations on the perfect and defective olivine systems, the optimised structures and energies of magnesium oxide and enstatite were also determined in order to compute the total energy change of a number of relevant defect reactions. For the calculations on the bulk phases, Monkhorst-Pack mesh sizes of  $6\times 6\times 6$  and  $2\times 3\times 5$  were utilised for MgO and enstatite, respectively. In the case of the olivine  $2\times 1\times 2$  supercell, reciprocal space was sampled only at the gamma point. While this leads to total energies that are not absolutely converged, the error in the energy differences is found to be less than 0.01 eV and therefore not significant with respect to thermal energy or the inherent uncertainties underlying density functional theory (*Ordejón et al.* [2001] and *Martin* [2004] give overviews of the accuracy of SIESTA and density functional theory, respectively).

The locations of the nuclei in each simulation box are moved in order to minimise the calculated energy of the system. Minimisation is performed using the method of conjugate gradients and convergence is assumed once the total force on each atom has become smaller than  $0.01 \text{ eV}\text{\AA}^{-1}$ . For the simulation cells containing defects, in order to simulate a dilute population of defects the cell parameters are held fixed at the values calculated for an equivalent defect free cell. Cell parameters of these perfect model crystals were varied as part of the energy minimisation and convergence was assumed when all components of the calculated stress tensor became smaller than 0.02 GPa. For calculations at high pressure we applied an isotropic external stress to the model crystal and optimised the

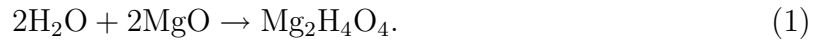
structure while allowing the cell parameters to vary. For defective forsterite the resulting smaller cell was used as the basis of the defective supercells, which were optimised with fixed cell parameters.

### 3. Results

#### 3.1. The Mg-vacancy and

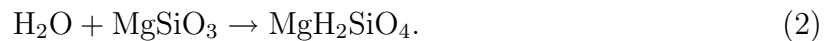
##### Si-vacancy Mechanisms

The first task is to identify the mechanisms of water incorporation in titanium-free forsterite in the system  $\text{MgO-SiO}_2\text{-H}_2\text{O}$ , *i.e.*, with no impurity species. Experimental work [Matveev *et al.*, 2001; Lemaire *et al.*, 2004] has shown that two mechanisms are observed, at low and high activity of silica, when the forsterite coexists with periclase ( $\text{MgO}$ ) or enstatite ( $\text{MgSiO}_3$ ), respectively. The first mechanism may be represented by the equilibrium:



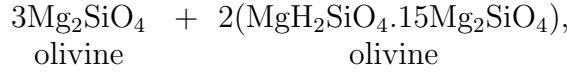
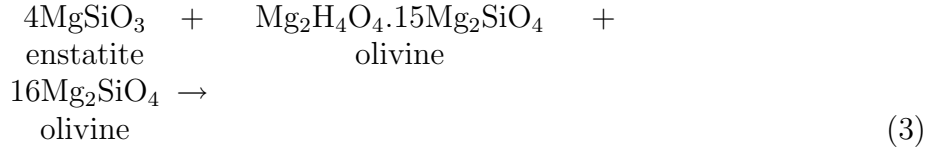
The hydrous component on the right hand side of the equation could have a point-defect structure similar to the hydrogrossular crystal structure, that is, a cluster of four hydroxyl groups around a silicon vacancy (Figure 2a). However, other point defects with the same stoichiometry are conceptually possible, for example, Mg occupying the silicon site with four protons associated with the vacated magnesium site. Furthermore, if local charge balance is not maintained, a huge variety of point-defect structures are conceptually possible, but such mechanisms seem unlikely and will not be pursued here.

The second mechanism may be represented by the equilibrium:

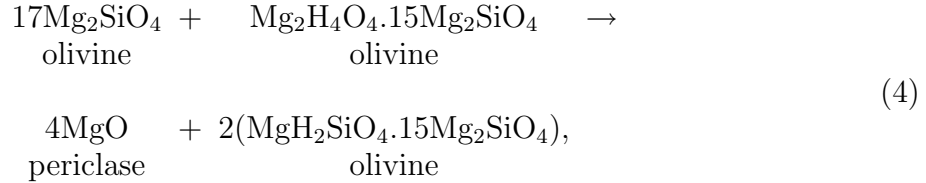


Here the hydrous component represents forsterite with Mg vacancies bound to two hydroxyl groups. Again this is not the only possible configuration with this stoichiometry, but other possibilities require Si to occupy a magnesium site and these have not been examined. We assume that the doubly protonated M1 vacancy with hydrogen bonded to the two O2 sites (Figure 2b) is the most stable hydrous configuration on the right hand side [*Wright and Catlow, 1994; Brodholt and Refson, 2000; Braithwaite et al., 2003*].

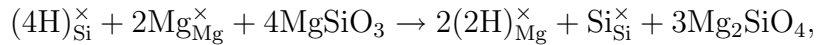
In order to explore the relative stability of these two defect configurations, without the complication of involving the energy of H<sub>2</sub>O as a component, the energetics of the reactions:



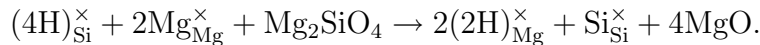
and:



were calculated for olivine in equilibrium with enstatite and MgO, respectively. These defect reactions can also be described using Kröger-Vink notation where vacancies are represented by a “V”, and the sites are represented by subscripts with reaction 3 described by:



and reaction 4 described by:



The energies for the two reactions are calculated using the total energies of the simulation cells presented in Table 1, which are designed to give the appropriate energy for isolated hydrous defects. Any residual defect - defect interactions will result in a lower dilution of the hydrous olivine component up to a maximum mole fraction of 1/16 (0.0625) for both hydrous components. The true dilution in the model system therefore lies between this value and the infinitely dilute isolated case. The calculation thus includes not only the energy of formation of the end-member defect, but also its heat of dilution in  $\text{Mg}_2\text{SiO}_4$  olivine. We assumed local charge balance, that is, that the hydrated cation vacancies are more stable than vacancies charge balanced by more distant hydroxyl groups, which is supported by previous calculations [*Wright and Catlow*, 1994; *Brodholt and Refson*, 2000; *Braithwaite et al.*, 2003; *Walker et al.*, 2006], and which is also consistent with the observation that the IR frequencies change with presumed vacancy type [*Matveev et al.*, 2001; *Lemaire et al.*, 2004; *Berry et al.*, 2005; *Matveev et al.*, 2005]. The energy changes are found to be 0.63 and 2.35 eV per defect, corresponding to 60  $\text{kJmol}^{-1}$  and 226  $\text{kJmol}^{-1}$  for reactions 3 and 4 respectively. Pressure has only a small effect on the enthalpy of reaction 3; at 12 GPa the equivalent reaction energy is found to be 58  $\text{kJmol}^{-1}$ . Pressure has a slightly larger effect on reaction 4 with the reaction energy changing to 242  $\text{kJmol}^{-1}$ .

In both cases, the reaction energies favour the formation of the hydrated silicon vacancy, a situation that does not accord with the experimental finding from IR spectroscopy that the type of defect varies with the coexisting phase. The explanation lies with the configurational entropy of the two types of defects. For the  $\text{MgH}_4\text{O}_4$  component (the Si vacancy with the hydrogrossular-like structure), four hydroxyl groups are associated with

the Si vacancy, and the configurational entropy is given by:

$$\begin{aligned}
 S_{\text{config}} &= k_B \ln \Omega \\
 &= k_B \left( \frac{(N_{\text{Mg}_2\text{SiO}_4} + N_{\text{Mg}_2\text{H}_4\text{O}_4})!}{N_{\text{Mg}_2\text{SiO}_4}! N_{\text{Mg}_2\text{H}_4\text{O}_4}!} \right) \\
 &= -R [X_{\text{Mg}_2\text{SiO}_4} \ln X_{\text{Mg}_2\text{SiO}_4} \\
 &\quad + X_{\text{Mg}_2\text{H}_4\text{O}_4} \ln X_{\text{Mg}_2\text{H}_4\text{O}_4}],
 \end{aligned} \tag{5}$$

where  $k_B$  is Boltzmanns constant,  $R$  is the gas constant,  $N_{\text{Mg}_2\text{SiO}_4}$  and  $N_{\text{Mg}_2\text{H}_4\text{O}_4}$  are the number of forsterite and hydrous-defect formula units in the crystal,  $X_{\text{Mg}_2\text{SiO}_4}$  and  $X_{\text{Mg}_2\text{H}_4\text{O}_4}$  is the mole fraction of formula units of the two components and  $\Omega$  is the configurational permutability. Note that this expression is for the integral molar configurational entropy, the partial molar configurational entropy,  $\bar{S}_{\text{config}}$ , of the  $\text{Mg}_2\text{H}_4\text{O}_4$  defect is:

$$\bar{S}_{\text{config}} = -R \ln X_{\text{Mg}_2\text{H}_4\text{O}_4}. \tag{6}$$

Similarly, for the  $\text{MgH}_2\text{SiO}_4$  component (the Mg-vacancy defect), we have assumed the two protons to be completely associated with the Mg vacancy, giving an integral molar configurational entropy:

$$\begin{aligned}
 S_{\text{config}} &= -R [X_{\text{Mg}_2\text{SiO}_4} \ln X_{\text{Mg}_2\text{SiO}_4} \\
 &\quad + X_{\text{MgH}_2\text{SiO}_4} \ln X_{\text{MgH}_2\text{SiO}_4}],
 \end{aligned} \tag{7}$$

and a partial molar configurational entropy:

$$\bar{S}_{\text{config}} = -R \ln X_{\text{MgH}_2\text{SiO}_4}. \tag{8}$$

The condition of equilibrium for a balanced chemical reaction is that the sum of the chemical potentials at constant composition is zero:

$$\sum \nu_i \mu_i = 0. \tag{9}$$

If we invoke the approximation that the calculated molar energy of the reaction is constant (*i.e.*, the change in heat capacity across the reaction is zero at all temperatures; this implies, *inter alia*, that the change in non-configurational or vibrational entropy across

the reaction is also zero), then we have:

$$\sum \nu_i \mu_i \cong \Delta E - T \sum \nu_i \overline{S}_{i,\text{config}} \quad (10)$$

Applying this condition to either reaction 3 or reaction 4, we obtain, for low concentrations of defects (*i.e.*,  $X_{\text{Mg}_2\text{SiO}_4} \approx 1$ ):

$$RT \ln \frac{(X_{\text{MgH}_2\text{SiO}_4})^2}{X_{\text{Mg}_2\text{H}_4\text{O}_4}} = -\Delta E. \quad (11)$$

This relation may be used to calculate the ratio of H<sub>2</sub>O held by the two types of defects; the important point is that this ratio is not a constant at a given T and P, but depends on the total amount of H<sub>2</sub>O dissolved in the olivine. The calculated ratio of water dissolved as MgH<sub>2</sub>SiO<sub>4</sub> to that dissolved as Mg<sub>2</sub>H<sub>4</sub>O<sub>4</sub>, *i.e.*,  $\frac{2X_{\text{MgH}_2\text{SiO}_4}}{X_{\text{Mg}_2\text{H}_4\text{O}_4}}$ , is plotted as a function of H<sub>2</sub>O content (calculated in ppm H<sub>2</sub>O, for convenience) in Figure 3, for two temperatures (1000°C and 1500°C) at the two activities of silica represented by reactions 3 (high  $a_{\text{SiO}_2}$ , in equilibrium with enstatite) and reaction 4 (low  $a_{\text{SiO}_2}$ , in equilibrium with periclase), respectively. The results show that when configurational entropy is taken into account, the Mg-vacancy mechanism (the MgH<sub>2</sub>SiO<sub>4</sub> component) is correctly predicted to be the more stable at high  $a_{\text{SiO}_2}$ .

This mechanism with its higher configurational entropy is of course also relatively stabilized by increasing temperature, but at constant temperature the low entropy mechanism (that involving Mg<sub>2</sub>H<sub>4</sub>O<sub>4</sub> component) becomes increasingly more important with increasing total H<sub>2</sub>O. High total H<sub>2</sub>O in olivine requires high  $f_{\text{H}_2\text{O}}$ , which is achieved in experiments by the presence of an H<sub>2</sub>O-rich vapour phase at high pressure. Such conditions are not usually possible in the chemically complex Earth's mantle (high  $f_{\text{H}_2\text{O}}$  would induce extensive melting), hence we emphasise that the results of simple-system experiments

on H<sub>2</sub>O-solubility in olivine conducted at saturation with H<sub>2</sub>O-vapour at high pressures cannot be applied directly to mantle olivine, although of course such data are needed to calibrate a thermodynamic model that takes into account the different mechanism of H<sub>2</sub>O substitution.

Our analysis correctly predicts that at intermediate  $f_{\text{H}_2\text{O}}$  (corresponding approximately to total H<sub>2</sub>O in olivine  $< 10^2$  ppm), either one mechanism or the other predominates according to whether  $a_{\text{SiO}_2}$  is buffered by MgO or MgSiO<sub>3</sub>, in agreement with the experimental results of *Matveev et al.* [2001] and *Lemaire et al.* [2004]. But at higher  $f_{\text{H}_2\text{O}}$  and greater H<sub>2</sub>O solubilities, such as those achieved in the experiments of *Kohlstedt et al.* [1996], the low  $a_{\text{SiO}_2}$  mechanism should become increasingly important even when the olivine is buffered by MgSiO<sub>3</sub>, again in agreement with the experimental observations (see *Kohlstedt et al.* [1996], their Figure 4).

### 3.2. Titanium incorporation in anhydrous forsterite

The FTIR spectra of typical olivines from the spinel-peridotite facies of the Earth's upper mantle is dominated not by either of these two defect mechanisms found in the system MgO-SiO<sub>2</sub>-H<sub>2</sub>O, but by a defect mechanism in which the OH<sup>-</sup> substitution is associated with Ti [*Berry et al.*, 2005]. In order to understand this mechanism, it is first necessary to discuss how Ti is incorporated in Mg<sub>2</sub>SiO<sub>4</sub> olivine without H<sub>2</sub>O.

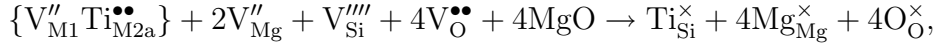
Three distinct types of mechanism have been considered: (i) direct substitution for silicon, (ii) substitution for magnesium charge balanced by a vacancy on an adjacent magnesium site, and (iii) substitution for magnesium charge balanced by a magnesium ion substitution onto an adjacent silicon site. Taking two polyhedra that share at least one

vertex oxygen atom as adjacent, there is one symmetry distinct arrangement for mechanism (i), nine distinct arrangements for mechanism (ii), and six distinct arrangements for mechanism (iii). The calculated energies of 112 and 111 atom simulation cells at 0 GPa containing these defect arrangements are listed in Table 2. When there is more than one arrangement of two adjacent defects (for example a vacancy on the M1 site with titanium on an M2 site, see Figure 4, the symmetry distinct arrangements are labelled with a lower case letter.

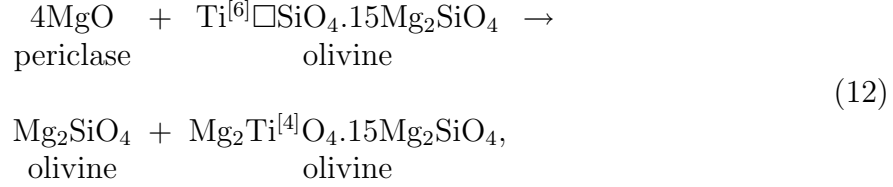
The content of the simulation cell is different for mechanisms (i) and (iii) from mechanism (ii). Comparing the energies of cells within each grouping reveals that titanium enters olivine via either direct substitution of silicon forming the  $\text{Ti}_{\text{Si}}^{\times}$  defect – the lowest energy configuration from mechanisms (i) and (iii), or via the coupled substitution  $\{\text{V}_{\text{M1}}\text{Ti}_{\text{M2a}}\}^{\times}$  – the lowest energy configuration from set (ii). As a forsterite crystal containing the  $\text{Ti}_{\text{Si}}^{\times}$  defect and any amount titanium will have different bulk chemistry to a crystal containing the  $\{\text{V}_{\text{M1}}\text{Ti}_{\text{M2a}}\}^{\times}$  defect and the same amount of titanium (for case (ii) the magnesium concentration will vary with titanium concentration, while in case (i) the silicon content will co-vary with titanium content), the preferred mechanism will depend on the chemistry of the crystal’s environment. This effect can be assessed by constructing relevant equilibria for the conversion of one defect to the other including the energy to digest or precipitate other oxides. The energies for a range of materials have been calculated and these are reported along with the lowest energy representative of each type of defective cell in Table 1. In an experiment where titanium bearing forsterite is in equilibrium with magnesium oxide the relevant reaction to convert one defect into the



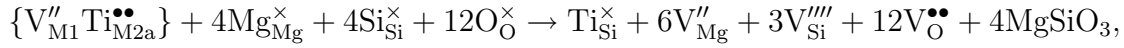
other can be written in Kröger-Vink notation as:



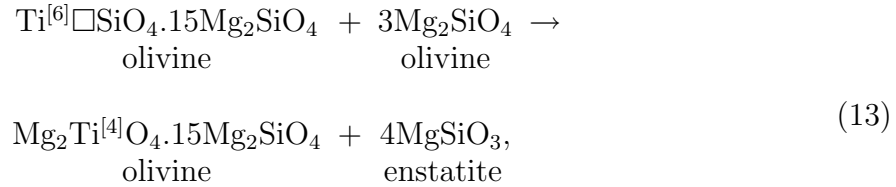
or as a reaction between chemical components:



which gives an energy of  $-169 \text{ kJmol}^{-1}$ , strongly favouring the direct substitution of titanium for silicon represented on the right hand side of this reaction. When there is no magnesium oxide to react and the titanium bearing forsterite is in equilibrium with orthopyroxene, which is the situation expected in the mantle, the reaction becomes:



in Kröger-Vink notation or:

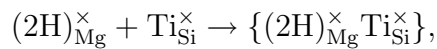


in terms of a reaction between components. This reaction gives an energy of  $-4 \text{ kJmol}^{-1}$ , weakly favouring the direct substitution of silicon for titanium although both substitution mechanisms are likely to be present. It is interesting to note that titanium bearing forsterite is predicted to be more stable in equilibrium with MgO compared with enstatite. This prediction is supported by the experimental study of *Hermann et al.* [2005], who found that titanium concentrations in olivine equilibrated with enstatite (low MgO activity) were four times lower than in experiments with olivine in equilibrium with spinel structured  $Mg_2TiO_4$  (high MgO activity). Figure 5 shows the results of these experiments

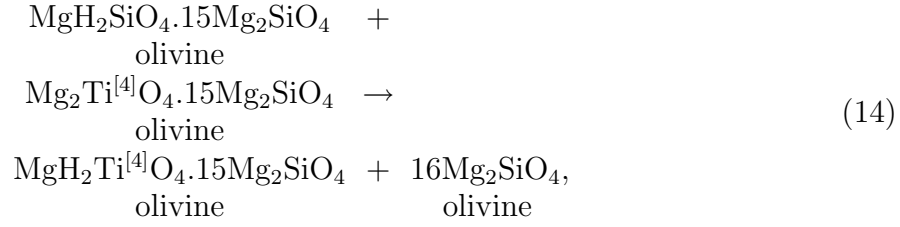
which indicate a dependence of Ti concentration on MgO activity. For substitution at 12 GPa, a pressure close to the forsterite – wadsleyite transition, we have only recalculated the energy of the lowest energy simulation cell for each mechanism found at 0 GPa (Table 1). Using these results we find that the direct substitution for silicon is destabilised by pressure and at 12 GPa the enthalpy change associated with reaction 13 is positive with a calculated energy of 55 kJmol<sup>-1</sup>.

### 3.3. The “titanium clinohumite” point defect

With the knowledge that hydrogen is likely to be incorporated as a doubly protonated magnesium vacancy at mantle temperatures and orthopyroxene-buffering in titanium-free forsterite, and that titanium is likely to be incorporated via the direct substitution for silicon in dry forsterite, we are now in a position to examine the coupled incorporation of titanium and hydrogen proposed by *Berry et al.* [2005]. Three kinds of substitutional mechanism are conceptually possible. The titanium and hydrogen point defects could be randomly distributed through the crystal, which would maximise the configurational entropy. The defects could be bound but with titanium still occupying the silicon site and the hydrogen ions occupying an adjacent magnesium vacancy. In the third possibility the defects react – the titanium ion moving from the silicon site into the vacant magnesium site and the two hydrogen ions moving from the magnesium site into the now vacant silicon site. To test to see if the second possibility is likely we evaluate the energy of the reaction:

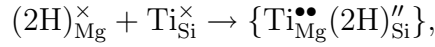


in Kröger-Vink notation or:

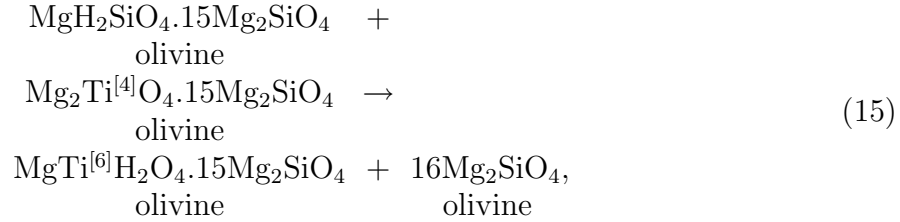


in terms of a reaction between components, giving an energy of  $-15 \text{ kJmol}^{-1}$  indicating that the defects are likely to be weakly bound.

The third possibility is evaluated via the reaction:

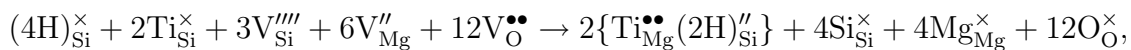


in Kröger-Vink notation or in terms of a reaction between components:

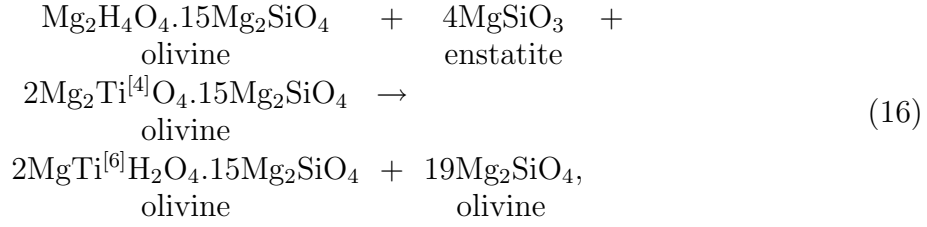


which gives an energy of  $-145 \text{ kJmol}^{-1}$  indicating that the reaction will occur. The fact that reaction 15 lowers the enthalpy more than reaction 14 shows that the exchange reaction (reaction 15) will be favored over the binding reaction (reaction 14). At 12 GPa the components on the right hand side of reaction 15 are further stabilised and the reaction enthalpy is found to be  $-217 \text{ kJmol}^{-1}$ . Assuming the effect of pressure is constant this gives a volume of this reaction as  $-6 \times 10^{-6} \text{ m}^{-3}\text{mol}^{-1}$ .

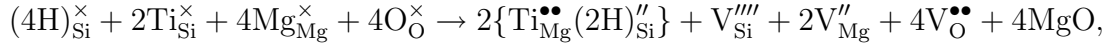
For completeness we finally consider the possibility of the reaction between hydrogen from a hydrogarnet type defect and titanium. Unlike reactions 14 and 15 this involves a change in the chemistry of the olivine crystal and thus depends on the buffer. For the system buffered by orthopyroxene the reaction is:



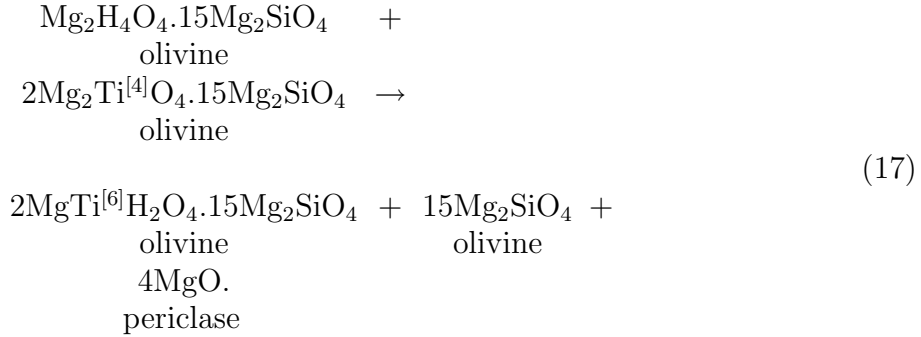
or:



while for an MgO buffered system the reaction is:



or:



The energy of reaction 16 is found to be -229 kJmol<sup>-1</sup> indicating that at mantle conditions the bound defect is also more stable than the isolated titanium and hydrogarnet defects. Again the hydrous titanium point defect is stabilised by pressure; at 12 GPa the reaction energy is found to be -316 kJmol<sup>-1</sup>. Reaction 17 is also favoured with a reaction energy of -64 kJmol<sup>-1</sup> at 12 GPa. The contribution to the free energy change associated with reactions 14, 15, 16 and 17 from the change in configurational entropy will favour the unbound titanium and hydrated cation vacancies.

An advantage of the calculations described here is that they not only provide information about the energies of defects but also the complete structure of the defects, including the titanium and hydrogen positions, that lead to these low energy configurations (e.g. Figure 6). Reactions 15, 16 and 17, at all pressures give the the lowest energy configuration consisting of a titanium ion occupying one of the small M1 sites located on an inversion

centre in the olivine structure. The M1 site is surrounded by two symmetry distinct pairs of silicon tetrahedra, one pair shares an O1 - O3 edge with the M1 octahedron while the second shares only the O2 vertex (Figure 4a). In the stable configuration, one of the edge sharing tetrahedra is occupied by two hydrogen ions rather than a silicon ion. The hydrogen ions are bonded to the two oxygen atoms that do not form part of the M1 octahedron containing the titanium ion (Figure 6a). In this way, all four oxygen atoms surrounding the vacant silicon site form covalent bonds (with hydrogen or with titanium) and the silicon vacancy is stabilised. Of the 30 symmetry distinct ways of arranging the ions in the titanium-clinohumite point defect (where Ti occupies a Mg site; see Figure 4 and Table 3) only two have all four oxygen ions around the silicon vacancy bonded to either titanium or hydrogen. The second arrangement has the titanium atom occupying an M2 site and the hydrogen ions bonded to O1 and O2 oxygen atoms (the two O3 atoms bond to the titanium). This arrangement is 0.45 eV less stable than the first arrangement with titanium on M1; while the driving force for this stabilisation cannot be determined directly from the calculations performed here, it is likely that the known preference for hydrogen to bond to O2 and O3 (rather than O1) atoms [*Wright and Catlow*, 1994; *Brodholt and Refson*, 2000; *Braithwaite et al.*, 2003; *Walker et al.*, 2006] plays a role. Other arrangements with at least one under-bonded oxygen atom are at least 0.5 eV (and typically more than 1 eV) less stable than the two fully bonded cases.

#### 4. Discussion

The results of the calculations presented above show that if water is incorporated into titanium bearing forsterite, composite defects will form that consist of a titanium ion occupying an M1 site adjacent to a silicon vacancy. Two of the four oxygen ions surrounding

the vacancy form covalent bonds with the titanium atom and the remaining two bond with hydrogen to form hydroxyl groups, thereby stabilising all four under bonded oxygen ions around the silicon vacancy. The existence of this configuration is supported by the results of IR and x-ray absorption near edge structure (XANES) spectroscopy [Berry *et al.*, 2005], also see Berry *et al.* [submitted]. The effect of this defect is to introduce silicon vacancies into the forsterite structure, which is expected to decrease its strength significantly.

#### 4.1. Comparison with experiment

The first evidence that our predicted structures are correct is provided by a comparison of the orientation of the O-H bonds from the calculations and the directions of maximum absorbance of IR radiation in experiments where the sample is orientated and the light is polarised. The IR spectra of the experimental samples of Lemaire *et al.* [2004] provide constraints on the hydrated cation vacancies formed in titanium free conditions. Their interpretation is that the IR bands between 3550 and 3650  $\text{cm}^{-1}$  are related to a silicon vacancy bound to hydroxyl groups and the measured absorbance is strongest when the electric vector is parallel to [100] and [001], compared to [010]. This pattern of polarisation would also be predicted from the calculated structure shown in Figure 2a, which has three of the four O-H bonds aligned nearly parallel to [100] and the fourth nearly parallel to [001]. The Lemaire *et al.* [2004] interpretation of the IR band close to 3160  $\text{cm}^{-1}$ , which is only observed in samples of high silica activity and when the electric vector is parallel to [001], is that this band is related to hydroxyl associated with magnesium vacancies in their sample. The calculated structure of this defect (Figure 2b) suggests that the polarisation direction should be in [001], in agreement with the experimental observation. We note that

the structure of the two defects has also been calculated by *Braithwaite et al.* [2003] and *Brodholt and Refson* [2000] using independent methods, both of which were different to the computational methodology used in this study. The structure of the magnesium vacancy – hydroxyl cluster is the same in all three cases but the details of the structure of the hydrogen – silicon vacancy clusters are different. *Braithwaite et al.* [2003] give polarisation directions due to O-H bonds around the silicon vacancy as being parallel to [100] and [010], and while *Brodholt and Refson* [2000] do not explicitly state the direction of the O-H bonds it is clear from their Figure 3 that an [010] component would be expected. Polarised IR spectra from the experimental titanium bearing samples of *Berry et al.* [2005] are not available due to the small sample size. However, we measured polarised IR spectra along the main axes of a San Carlos olivine cube (Figure 1). This olivine displays the typical Ti-OH fingerprint identified by *Berry et al.* [2005]. The polarised spectra show the strongest absorption when the electric vector is parallel to the [100] direction, about a factor of ten less absorption when the vector is parallel to [001] and essentially no absorption when the vector is parallel to [010] (Figure 1). This is exactly the polarisation behaviour that would be expected for the most stable defect containing both hydrogen and titanium shown in Figure 6a, which has O-H bonds in the (010) plane. It is important to note that Ti-free olivine that has four  $\text{OH}^{-1}$  groups surrounding silica vacancies (Figure 2a) displays a very similar polarisation behavior and thus the two Si-defect types cannot be distinguished using this approach. However, the comparison between the calculated positions of the O-H bonds with polarised infra red spectroscopy provides strong evidence that H decorating a Si or a Mg vacancy can be distinguished. This approach confirms earlier suggestions that IR bands in the region of  $3612\text{--}3525\text{ cm}^{-1}$  are related to Si vacancies and the broad

peaks at 3220-3160  $\text{cm}^{-1}$  are related to Mg vacancies [*Lemaire et al.*, 2004; *Berry et al.*, 2005]

Additional experimental constraints also support the results of the simulations presented above. Most obviously, the IR spectrum of the hydrated titanium defect is similar to the IR spectrum for forsterite equilibrated with MgO (see Figure 1). If the assumption that the high wavenumber MgO equilibrated fingerprint corresponds to a hydrated silicon vacancy is correct, an assumption that is strongly supported by the calculated IR frequencies of *Braithwaite et al.* [2003], then the similarity between the two fingerprints reflects the similar structure found in the two defects. Further supporting results relate to the mechanism of titanium incorporation in hydrogen free forsterite. The incorporation mechanism has been examined by *Hermann et al.* [2005] who found that the titanium concentration in hydrogen free olivine equilibrated in the presence of rutile co-varies with the concentration of silicon in the sample while the concentration of magnesium is independent of the titanium content (Figure 5). This supports the view that titanium incorporation should occur via substitution of titanium for silicon as proposed above. Extended x-ray absorption fine structure (EXAFS) spectroscopy is also consistent with this model, with experimentally determined Ti-O bond lengths being in good agreement with the structure derived from calculation. The calculated bond lengths for titanium on the magnesium sites are significantly too long to reconcile with the EXAFS results [*Berry et al.*, submitted].

The XANES results reported by *Berry et al.* [2005] are also in agreement with the calculated structure of the defects. These experiments use the energy and intensity of the  $1s \rightarrow 3d$  pre-edge peak in the K-edge absorption spectrum to determine the co-ordination



number of titanium from an empirical correlation. In particular, the XANES spectrum of hydrogen free olivine shows the presence of tetrahedrally co-ordinated titanium while the spectrum of hydrated titanium bearing olivine shows the presence of octahedrally co-ordinated titanium. Thus XANES experiments strongly support the conclusion that a mechanism like reaction 15 is energetically favoured.

## 4.2. Diffusion and water weakening

The results of the calculations provide an atomic scale view of the naturally occurring hydrogen defects in olivine, which permits conclusions about the effect of hydrogen on, for example, electrical conductivity and cation mobility, to be assessed. Of crucial importance for the physical properties of olivine is the presence of a silicon vacancy in the proposed titanium-clinohumite point defect cluster. However, the situation is complicated as there is no completely accepted model that relates the diffusivity of the constituents of a chemically complex ionic material to its creep rate. The standard model, that diffusion of the most slowly moving species moving by the most rapid pathway limits creep [*Poirier*, 1985], works well in binary oxides deforming by bulk diffusion and grain boundary sliding, or by dislocation climb, but is less successful in the case of olivine. For example, typical activation energies for anhydrous polycrystalline olivine deforming by a dislocation climb limited process are  $\sim 510 \text{ kJmol}^{-1}$  [e.g. *Mei and Kohlstedt*, 2000b] with activation volumes that vary between  $6 \times 10^{-6}$  and  $27 \times 10^{-6} \text{ m}^3\text{mol}^{-1}$  [see the review of *Hirth and Kohlstedt*, 2003]. The fact that silicon is the most slowly diffusing species in olivine was established by *Houlier et al.* [1988] and there are experimental studies that report activation energies and volumes. *Houlier et al.* [1990] found a much lower activation energy for silicon diffusion ( $291 \text{ kJmol}^{-1}$ ) than the activation energy for creep. Later experiments to extract the

activation volume for silicon diffusion gave results close to  $0 \text{ m}^3\text{mol}^{-1}$  [Béjina *et al.*, 1997, 1999], also significantly different from the observed pressure effect for creep. An attempt to rigourously explain these differences was made by Jaoul [1990] who could reconcile them by requiring that the driving force for diffusion consisted of a gradient in the chemical potential and electrostatic interactions between diffusing defects. However, later experiments recovered an activation energy for silicon diffusion of  $529 \pm 41 \text{ kJmol}^{-1}$  – within error of the activation energy for creep [Dohmen *et al.*, 2002]. It is unclear if new experiments at high pressure would result in a change in the activation volume for diffusion and invalidate the model of Jaoul [1990], but whatever the correct model for the deformation of olivine is, it seems most likely that silicon diffusion will play a major role. With this in mind the most probable model for water weakening in forsterite is for water incorporation to increase the number of silicon vacancies in the crystal.

The critical importance of silicon vacancies in relation to the water weakening mechanism was recognised by Brodholt and Refson [2000], who showed that hydrogen acts to lower the formation energy of silicon and magnesium vacancies. At any temperature this would lead to more intrinsic defects than would be present in a hydrogen free crystal, leading to a water weakening effect. However, at most temperatures the expectation is that the defect population in natural olivine will be dominated by extrinsic defects formed by the incorporation of impurities. For the titanium free system adding water is likely to increase the number of magnesium vacancies and not directly alter the number of silicon vacancies. In the titanium bearing system the addition of water directly increases the concentration of silicon vacancies – for each absorbed molecule of water there will be one additional silicon vacancy as long as there is sufficient titanium to act as an agent for its

stabilisation. The diffusivity of silicon is therefore expected to be directly proportional to the amount of incorporated water allowing very significant water weakening.

A related problem is the effect of the proposed titanium-hydrogen point defect on the atomic scale diffusion mechanism of silicon in olivine. If the mechanism for the diffusion of silicon vacancies or interstitial ions in pure forsterite is significantly different from the mechanism for diffusion of the silicon vacancy in the hydrated point defect described here, it is likely that the energetic barrier to point defect migration and thus the activation energy for diffusion will be different in the two cases. Although the evaluation of the activation energy for diffusion from atomic scale simulation is possible [*Walker et al.*, 2003; *Jaoul et al.*, 1995], the computational resources required are significantly in excess of those needed for identifying the structure and energies of stable and metastable point defects and we have not attempted such calculations for the proposed defect. However, it seems probable that any diffusion pathway would involve some of the metastable configurations for the titanium-hydrogen point defect identified in table 3. If this is the case it is possible to place a *lower bound* on the activation energy for diffusion equal to the difference in energy between the lowest energy stable configuration and higher energy metastable configurations. Depending on which defect configurations are chosen as the metastable state this limit is between 50 and 150 kJmol<sup>-1</sup>, significantly less than the energy required to form an intrinsic silicon vacancy [*Braithwaite et al.*, 2003]. This may partially explain the influence of water on silicon diffusion recently reported by *Chakraborty and Costa* [2004].

## 5. Conclusions

The calculations indicate that: (i) At low pressure, the most stable configuration for titanium in anhydrous forsterite is a direct substitution for silicon; this is supported by XANES and EXAFS data. (ii) The most stable configuration for cations and hydrogen in titanium-free forsterite coexisting with pyroxene is the formation of hydrated magnesium vacancies on the smaller of the two magnesium sites. (iii) The reaction of titanium and the hydrated cation vacancy is thermodynamically favoured, and results in the formation of a cluster of point defects with six-coordinated titanium on a magnesium site adjacent to a vacant silicon site containing two hydrogen ions. As silicon is the most slowly diffusing species in olivine, increasing the number of silicon vacancies is expected to lead to a weakening of olivine in the dislocation climb and diffusion creep deformational regimes. The process outlined above will lead to an increase in the number of silicon vacancies in olivine as hydrogen is incorporated into the crystal and thus amounts to a novel and credible explanation for the observed water weakening of olivine. Furthermore, the results of the computer calculations are in agreement with a wide range of experimental observations. As well as the results of x-ray and IR spectroscopy outlined above, the mechanism is consistent with the dependance of water solubility on oxygen partial pressure found for “group I” bands by *Bai and Kohlstedt* [1993]. These bands were found to vary with the  $\sim 1/6$  power of the oxygen partial pressure and according to the point defect models of *Stocker and Smyth* [1977], this indicates that hydrogen incorporation is either charge balanced by magnesium vacancies or oxygen interstitials. Because reactions such as reaction 15 do not change the stoichiometry of the crystal (they only rearrange the position of the defects), the dependance of hydrogen solubility with oxygen partial pressure is unaffected

by the action of our proposed incorporation mechanism; the dependence is not changed by the presence of titanium.

Finally, we note that our results are expected to hold for all upper mantle pressures. However, samples synthesised at pressures greater than 5 GPa show IR bands that are not explained by the Ti-mechanism suggested here [Kohlstedt *et al.*, 1996] and correspond to the signature of hydrated silicon vacancies identified by Matveev *et al.* [2001], Lemaire *et al.* [2004] and Berry *et al.* [2005]. Indeed Berry *et al.* [2005] suggests that while water is incorporated at the hydrated Ti point defect in olivine from spinel peridotite, the hydrated silicon vacancy becomes more important with increasing pressure. Although we do not predict a major pressure induced change in the relative stability of the hydrated silicon vacancy compared to either the hydrated magnesium vacancy (Reactions 3 and 4) or the hydrated titanium point defect (Reactions 16 and 17) with pressure, this does not rule out the possibility of an increase in the stability of this defect as the pressure and temperature conditions approach the stability field of a hydrous phase (such as OH-clinohumite). Such an increase in stability could alter the relative stability of any of the classes of defects examined here at very high pressure. Alternatively, at higher  $f_{\text{H}_2\text{O}}$  and greater  $\text{H}_2\text{O}$  solubilities the hydrated silicon vacancy could be stabilized by the entropic effects discussed in section 3.1, even when the olivine is buffered by  $\text{MgSiO}_3$ .

**Acknowledgments.** We thank the Australian Partnership for Advanced Computing and the Centre for Advanced Data Inference for access to high performance computer facilities. JH and AJB acknowledge financial support from the Australian Research Council.

## References

- Bai, Q., and D. L. Kohlstedt (1993), Effects of chemical environment on the solubility and incorporation mechanism for hydrogen in olivine, *Physics and Chemistry of Minerals*, *19*, 460 – 471.
- Béjina, F., P. Raterron, J. Zhang, O. Jaoul, and R. C. Liebermann (1997), Activation volume of silicon diffusion in San Carlos olivine, *Geophysical Research Letters*, *24*, 2597 – 2600.
- Béjina, F., O. Jaoul, and R. C. Liebermann (1999), Activation volume of Si diffusion in San Carlos olivine: implications for upper mantle rheology, *Journal of Geophysical Research*, *104*, 25,529–25,542.
- Bell, D. R., G. R. Rossman, J. Maldener, D. Endisch, and F. Rauch (2003), Hydroxide in olivine: A quantitative determination of the absolute amount and calibration of the IR spectrum, *Journal of Geophysical Research*, *108*, doi:10.1029/2001JB000679.
- Berry, A. J., J. Hermann, H. St. C. O'Neill, and G. J. Foran (2005), Fingerprinting the water site in mantle olivine, *Geology*, *33*, 869 – 872.
- Berry, A. J., A. M. Walker, J. Hermann, H. St. C. O'Neill, G. J. Foran, and J. D. Gale (submitted), Titanium substitution mechanisms in forsterite, submitted to *Chemical Geology*.
- Braithwaite, J. S., K. Wright, and C. R. A. Catlow (2003), A theoretical study of the energetics and IR frequencies of hydroxyl defects in forsterite, *Journal of Geophysical Research Solid Earth*, *108*, 2284, doi:10.1029/2002JB002126.
- Brodholt, J. P., and K. Refson (2000), An ab initio study of hydrogen in forsterite and a possible mechanism for hydrolytic weakening, *Journal of Geophysical Research*, *105*,

18,977 – 18,982.

Chakraborty, S., and F. Costa (2004), Fast diffusion of Si and O in san carlos olivine under hydros conditions, *Geochimica et Cosmochimica Acta*, 68, A275.

Dohmen, R., S. Chakraborty, and H.-W. Becker (2002), Si and O diffusion in olivine and implications for characterizing plastic flow in the mantle, *Geophysical Research Letters*, 29, 2030.

Evans, R. L., P. Tarits, A. D. Chave, A. White, G. Heinson, J. H. Filloux, H. Toh, N. Seama, H. Utada, J. R. Booker, and M. J. Unsworth (1999), Asymmetric electrical structure in the mantle beneath the East Pacific Rise at 17°S, *Science*, 289, 752 – 756.

Gatzemeier, A., and M. Moorkamp (2005), 3D modelling of electrical anisotropy from electromagnetic array data: hypothesis testing for different upper mantle conduction mechanisms, *Physics of the Earth and Planetary Interiors*, 149, 225–242.

Hermann, J., H. S. O'Neill, and A. J. Berry (2005), Titanium solubility in olivine in the system  $\text{TiO}_2\text{-MgO-SiO}_2$ : no evidence for an ultra-deep origin of Ti-bearing olivine, *Contributions to Mineralogy and Petrology*, 148, 746–760.

Hirth, G., and D. Kohlstedt (2003), Rheology of the upper mantle and the mantle wedge: A view from the experimentalists, in *Microscopic Properties and Processes in Minerals*, *Geophysical Monograph Series*, vol. 138, edited by J. Eiler, pp. 83 – 105, AGU.

Hohenberg, P., and W. Kohn (1964), Inhomogeneous electron gas, *Physical Review*, 136, 864 – 871.

Houlier, B., O. Jaoul, F. Abel, and R. C. Liebermann (1988), Oxygen and silicon self-diffusion in natural olivine, *Physics of the Earth and Planetary Interiors*, 50, 240 – 250.

- Houlier, B., M. Cheraghmakani, and O. Jaoul (1990), Silicon diffusion in San Carlos olivine, *Physics of the Earth and Planetary Interiors*, *62*, 329 – 340.
- Jaoul, O. (1990), Multicomponent diffusion and creep in olivine, *Journal of Geophysical Research*, *95*, 17,631 – 17,642.
- Jaoul, O., Y. Bertran-Alvarez, R. C. Liebermann, and G. D. Price (1995), Fe-Mg interdiffusion in olivine up to 9 GPa at  $T = 600\text{--}900^\circ\text{C}$ ; experimental data and comparison with defect calculations, *Physics of the Earth and Planetary Interiors*, *89*, 199 – 218.
- Junquera, J., O. Paz, D. Sánchez-Portal, and E. Artacho (2001), Numerical atomic orbitals for linear-scaling calculations, *Physical Reviews B*, *64*, 235,111.
- Karato, S.-I. (1990), The role of hydrogen in the electrical conductivity of the upper mantle, *Nature*, *347*, 272 – 273.
- Karato, S.-I., and H. Jung (1998), Water, partial melting and the origin of the seismic low velocity and high attenuation zone in the upper mantle, *Earth and Planetary Science Letters*, *157*, 193 – 207.
- Kaula, W. M. (1990), Venus: A contrast in evolution to Earth, *Science*, *247*, 1191 – 1196.
- Kaula, W. M. (1995), Venus reconsidered, *Science*, *270*, 1460 – 1464.
- Koch-Müller, M., S. S. Matsyuk, D. Rhede, R. Wirth and N. Khisina (2006) Hydroxyl in mantle olivine xenocrysts from the Udachnaya kimberlite pipe, *Physics and Chemistry of Minerals*, *33*, 276 – 287.
- Kohlstedt, D. L., H. Keppler, and D. C. Rubie (1996), Solubility of water in the alpha, beta and gamma phases of  $(\text{MgFe})_2\text{SiO}_4$ , *Contributions to Mineralogy and Petrology*, *123*, 345 – 357.



- Kohn, W., and L. J. Sham (1965), Self-consistent equations including exchange and correlation effects, *Physical Review*, *140*, 1133 – 1138.
- Lemaire, C., S. C. Kohn, and R. A. Brooker (2004), The effect of silica activity on the incorporation mechanisms of water in synthetic forsterite: a polarized infrared spectroscopic study, *Contributions to Mineralogy and Petrology*, *147*, 48 – 57.
- Lizarralde, D., A. Chave, G. Hirth, and A. Schultz (1995), Northeastern Pacific mantle conductivity profile from long-period magnetotelluric sounding using Hawaii-to-California submarine cable data, *Journal of Geophysical Research*, *100*, 17,837 – 17,854.
- Martin, R. M. (2004), *Electronic structure basic theory and practical methods*, Cambridge University Press, Cambridge.
- Matsyuk, S. S. and K. Langer (2004), Hydroxyl in olivines from mantle xenoliths in kimberlites of the Siberian platform, *Contributions to Mineralogy and Petrology*, *147*, 413 – 437.
- Matveev, S., H. St. C. O'Neill, C. Ballhaus, W. R. Taylor, and D. H. Green (2001), Effect of silica activity on OH<sup>-</sup> IR spectra of olivine: implications for low-aSiO<sub>2</sub> mantle metasomatism, *Journal of Petrology*, *42*, 721 – 729.
- Matveev, S., M. Potnyagin, C. Ballhaus, R. A. Brooker, and C. A. Geiger (2005), FTIR spectrum of phenocryst olivine as an indicator of silica saturation in magmas, *Journal of Petrology*, *46*, 605 – 614.
- Mei, S., and D. L. Kohlstedt (2000a), Influence of water on plastic deformation of olivine aggregates, 1. diffusion creep regime, *Journal of Geophysical Research*, *105*, 21,457 – 21,469.

- Mei, S., and D. L. Kohlstedt (2000b), Influence of water on plastic deformation of olivine aggregates, 2. dislocation creep regime, *Journal of Geophysical Research*, *105*, 21,471 – 21,481.
- Ordejón, P., E. Artacho, R. Cachau, J. Gale, A. García, J. Junquera, J. Kohanoff, M. Machado, D. Sánchez-Portal, J. M. Soler, and R. Weht (2001), Linear scaling DFT calculations with numerical atomic orbitals, *Materials Research Society Symposium Proceedings*, *677*, AA9.6.1 – AA9.6.12.
- Perdew, J. P., K. Burke, and M. Ernzerhof (1996), Generalized gradient approximation made simple, *Physical Review Letters*, *77*, 3865 – 3868.
- Poirier, J.-P. (1985), *Creep of crystals. High-temperature deformation processes in metals, ceramics and minerals*, Cambridge Earth sciences series, Cambridge University Press, Cambridge.
- Regenauer-Lieb, K., and T. Kohl (2003), Water and diffusivity in olivine: its role in planetary tectonics, *Mineralogical Magazine*, *67*, 697 – 715.
- Regenauer-Lieb, K., D. A. Yuen, and J. Branlund (2001), The initiation of subduction: criticality by addition of water?, *Science*, *294*, 578 – 580.
- Richmond, N. C., and J. P. Brodholt (2000), Incorporation of  $\text{Fe}^{3+}$  into forsterite and wadsleyite, *American Mineralogist*, *85*, 1155–1158.
- Soler, J. M., E. Artacho, J. D. Gale, A. García, J. Junquera, P. Ordejón, and D. Sánchez-Portal (2002), The siesta method for ab initio order- $N$  materials simulation, *Journal of Physics: Condensed Matter*, *14*, 2745 – 2776.
- Solomon, S. C., J. W. Head, W. M. Kaula, D. McKenzie, B. Parsons, R. J. Phillips, G. Schubert, and M. Talwani (1991), Venus tectonics initial analysis from Magellan,

*Science*, 252, 297 – 321.

Stocker, R. L., and D. M. Smyth (1977), Effect of enstatite activity and oxygen partial pressure on the point-defect chemistry of olivine, *Physics of the Earth and Planetary Interiors*, 16, 145–156.

Walker, A. M., K. Wright, and B. Slater (2003), A computational study of oxygen diffusion in olivine, *Physics and Chemistry of Minerals*, 30, 536 – 545.

Walker, A. M., S. Demouchy, and K. Wright (2006), Computer modelling of the energies and vibrational properties of hydroxyl groups in  $\alpha$ - and  $\beta$ -Mg<sub>2</sub>SiO<sub>4</sub>, *European Journal of Mineralogy*, 18, 529 – 543.

Wang, D., M. Mookherjee, Y. Xu, and S.-I. Karato (2006), The effect of water on the electrical conductivity of olivine, *Nature*, 443, 977 – 980.

Wright, K., and C. R. A. Catlow (1994), A computer simulation study of (OH) defects in olivine, *Physics and Chemistry of Minerals*, 20, 515 – 518.


Yoshino, T., T. Matsuzaki, S. Yamashita, and T. Katsura (2006), Hydrous olivine unable to account for conductivity anomaly at the top of the asthenosphere, *Nature*, 443, 973 – 976.

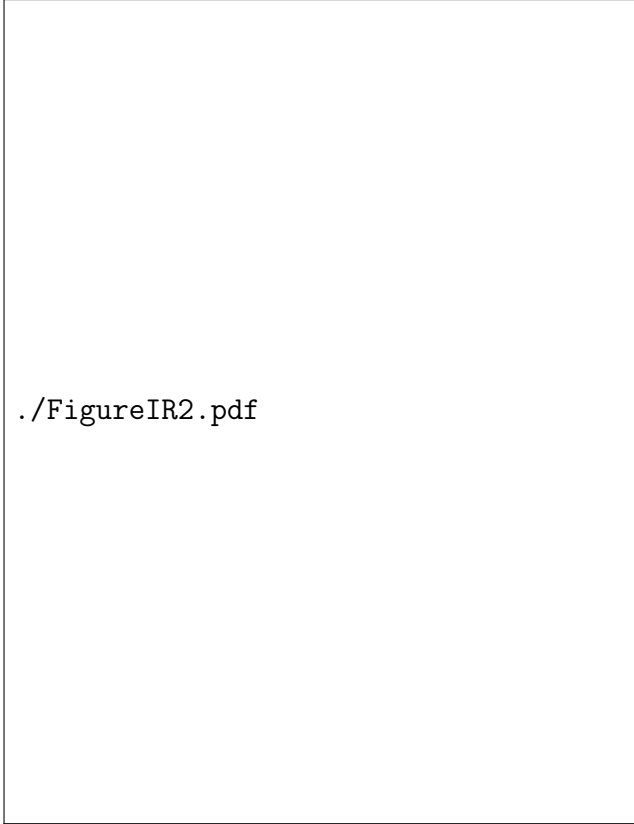


**Figure 1.** Unpolarized and polarized infra-red spectra of San Carlos olivine and unpolarized olivine spectra from experimental runs. The proposed stable hydrous defects is indicated for the experimental olivine spectra (Fo = forsterite, Rt = rutile, Per = periclase, En = enstatite).

**Table 1.** Low energy simulation cells used in this study

Simulation cell	Calculated formation energy (eV)	
	0 GPa	12GPa
$\text{Mg}_2\text{SiO}_4$	-3905.55	-3905.33
$\text{MgSiO}_3$	-2444.02	-2443.86
$\text{MgO}$	-1461.10	-1460.99
$\text{Mg}_2\text{Ti}^{[4]}\text{O}_4.15\text{Mg}_2\text{SiO}_4$	-63967.17	-63962.82
$\text{Ti}^{[6]}\square\text{SiO}_4.15\text{Mg}_2\text{SiO}_4$	-62026.56	-62022.84
$\text{MgTi}^{[6]}\text{Mg}^{[4]}\text{O}_4.15\text{Mg}_2\text{SiO}_4$	-63965.49	-63961.14
$\text{MgH}_2\text{SiO}_4.15\text{Mg}_2\text{SiO}_4$	-61494.75	-61490.94
$\text{Mg}_2\text{H}_4\text{O}_4.15\text{Mg}_2\text{SiO}_4$	-62441.90	-62437.75
$\text{MgH}_2\text{Ti}^{[4]}\text{O}_4.15\text{Mg}_2\text{SiO}_4$	-63973.28	-62969.10
$\text{MgTi}^{[6]}\text{H}_2\text{O}_4.15\text{Mg}_2\text{SiO}_4$	-62974.63	-62970.74



./cationvacs.pdf

**Figure 2.** Structure of stable hydrated cation vacancies derived from DFT calculations. (a) Fully hydrated silicon vacancy, three of the OH dipoles are aligned sub-parallel to the [100] direction and the fourth is sub-parallel to the [001] direction. (b) Hydrated M1 vacancy with hydrogen bonded to two O2 oxygen atoms, both OH dipoles are sub-parallel to the [001] direction with small resolved components in the [010] direction. Hydrogen atoms in black and silicon atoms in light grey are shown bonded to oxygen atoms (in part (a) four isolated OH groups are at the corners of a vacant Si tetrahedra). Isolated atoms in part (a) are magnesium atoms, these are omitted from part (b).

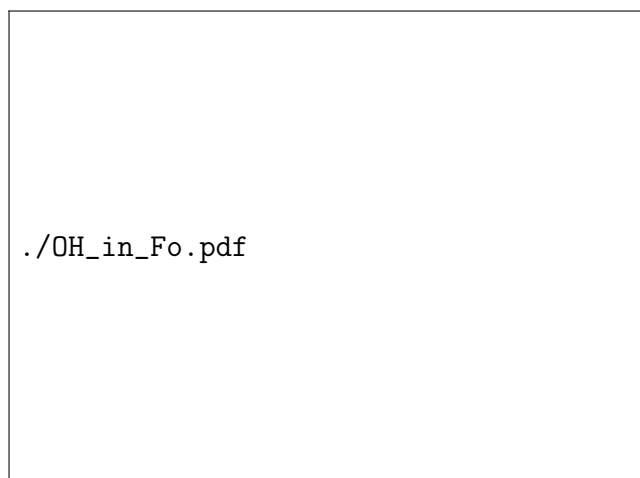


**Figure 3.** Ratio of  $\text{H}_2\text{O}$  substituting in  $\text{MgH}_2\text{SiO}_4$  defects (Mg vacancies) to that substituting in  $\text{Mg}_2\text{H}_4\text{O}_4$  defects (Si vacancies) as a function of total  $\text{H}_2\text{O}$ , (*i.e.*,  $X_{\text{MgH}_2\text{SiO}_4} + 0.5X_{\text{Mg}_2\text{H}_4\text{O}_4}$ , but expressed as parts per million (ppm)  $\text{H}_2\text{O}$ ). The ratios are calculated at two temperatures,  $1000^\circ\text{C}$  and  $1500^\circ\text{C}$ , for high  $a_{\text{SiO}_2}$  ( $\text{MgSiO}_3$ -saturated, reaction 3) and low  $a_{\text{SiO}_2}$  (reaction 4).

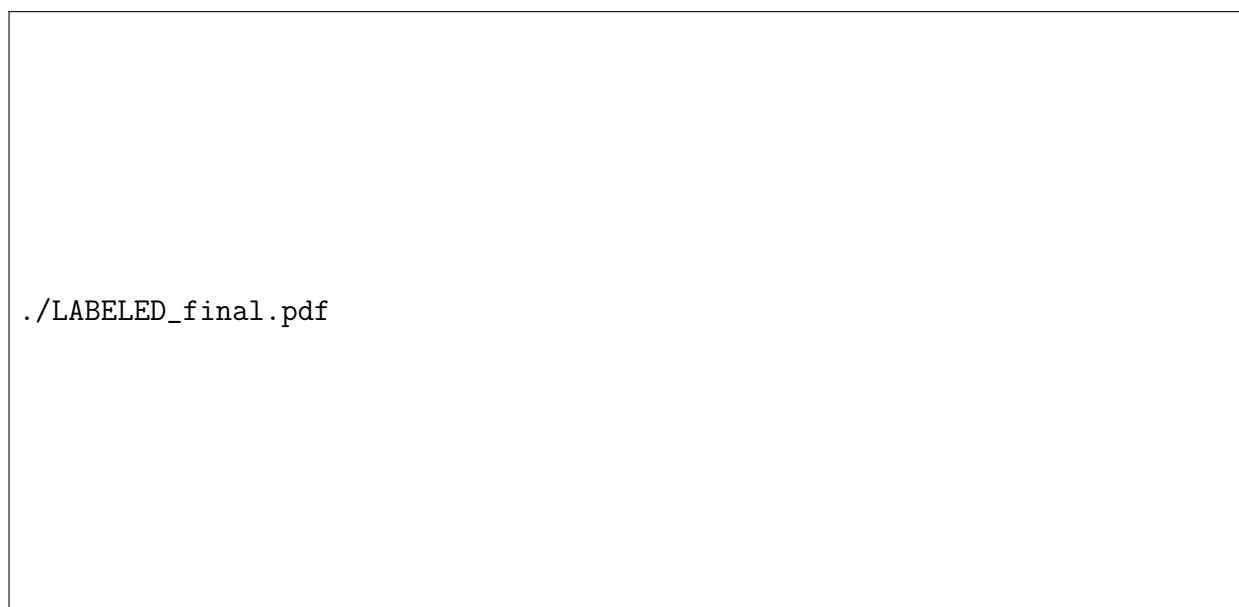
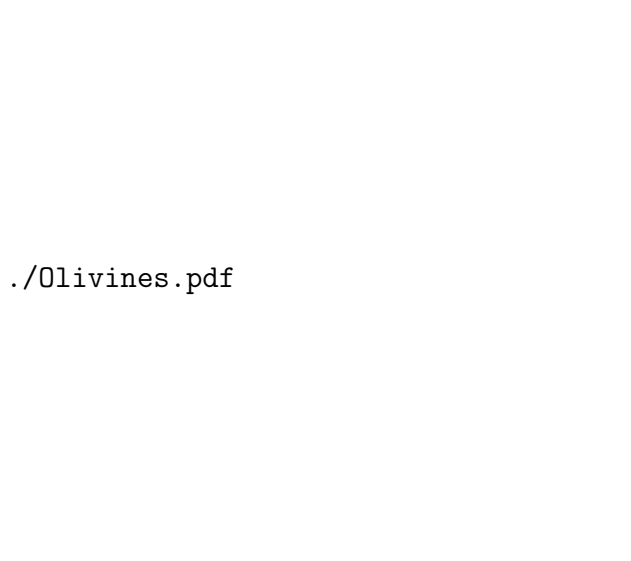


**Figure 4.** Structure of the two magnesium sites and surrounding silicon tetrahedra in forsterite. (a) M1 site surrounded by two pairs of inequivalent tetrahedra, atom types are marked and letters in parentheses indicate atoms on the same symmetry position that are not equivalent from the point of view of the central M1 site. (b) M2 site surrounded by five tetrahedra.



./Olivines.pdf

**Figure 5.** Composition of experimental titanium bearing olivine samples (Ol = olivine, Per = periclase, En = enstatite) equilibrated at 1400°C and 1 atm. The line indicates the expected relationship if incorporation occurs by the replacement of silicon with titanium.

**Table 2.** Defect energies for all titanium defects in dry forsterite

Defect	Energy (eV)
$\text{Ti}_{\text{Si}}^{\times}$	-63967.17
$\{\text{V}_{\text{M1}}'' \text{Ti}_{\text{M1}}^{\bullet\bullet}\}$	-62026.20
$\{\text{V}_{\text{M1}}'' \text{Ti}_{\text{M2(a)}}^{\bullet\bullet}\}$	-62026.56
$\{\text{V}_{\text{M1}}'' \text{Ti}_{\text{M2(b)}}^{\bullet\bullet}\}$	-62026.21
$\{\text{V}_{\text{M1}}'' \text{Ti}_{\text{M2(c)}}^{\bullet\bullet}\}$	-62026.22
$\{\text{V}_{\text{M2}}'' \text{Ti}_{\text{M1(a)}}^{\bullet\bullet}\}$	-62024.55
$\{\text{V}_{\text{M2}}'' \text{Ti}_{\text{M1(b)}}^{\bullet\bullet}\}$	-62024.58
$\{\text{V}_{\text{M2}}'' \text{Ti}_{\text{M1(c)}}^{\bullet\bullet}\}$	-62024.91
$\{\text{V}_{\text{M2}}'' \text{Ti}_{\text{M2(a)}}^{\bullet\bullet}\}$	-62024.86
$\{\text{V}_{\text{M2}}'' \text{Ti}_{\text{M2(b)}}^{\bullet\bullet}\}$	-62024.89
$\{\text{Ti}_{\text{M1}}^{\bullet\bullet} \text{Mg}_{\text{Si(a)}}''\}$	-63965.49
$\{\text{Ti}_{\text{M1}}^{\bullet\bullet} \text{Mg}_{\text{Si(b)}}''\}$	-63963.97
$\{\text{Ti}_{\text{M2}}^{\bullet\bullet} \text{Mg}_{\text{Si(a)}}''\}$	-63964.68
$\{\text{Ti}_{\text{M2}}^{\bullet\bullet} \text{Mg}_{\text{Si(b)}}''\}$	-63964.73
$\{\text{Ti}_{\text{M2}}^{\bullet\bullet} \text{Mg}_{\text{Si(c)}}''\}$	-63964.20
$\{\text{Ti}_{\text{M2}}^{\bullet\bullet} \text{Mg}_{\text{Si(d)}}''\}$	-63965.32

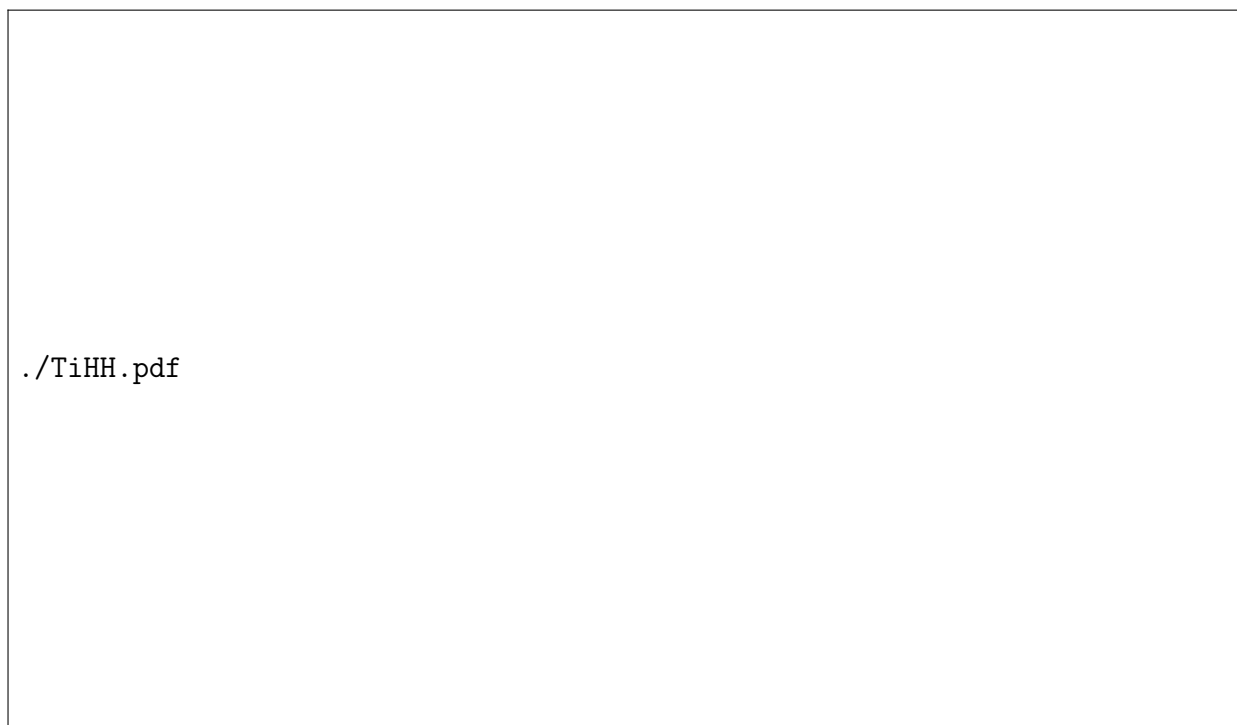


**Figure 6.** Structure of hydrated titanium defect. (a) Stable defect with titanium on the M1 site next to a silicon vacancy containing two hydrogen atoms, both OH dipoles have strong resolved components in the  $[100]$  direction and smaller components in the  $[001]$  direction. (b) Less stable defect with titanium on the silicon site next to a hydrated M1 vacancy similar to that shown in Figure 2b, note the lengthening of the Ti–O bonds compared to the Si–O bonds. Atom types are given in Figure 4, hydrogen atoms are black and titanium atoms are marked.



**Table 3.** Total energies for all “titanium-clinohumite” defect containing simulation cells in

forsterite. The structure of the cells marked with an asterisk are shown in Figure 6

Defect	Energy (eV)
$\{\text{Ti}_{\text{M2}}^{\bullet\bullet} \text{V}_{\text{Si(a)}}^{\bullet\bullet\bullet\bullet} \text{OH}_{\text{O1}}^{\bullet} \text{OH}_{\text{O2}}^{\bullet}\}$	-62973.43
$\{\text{Ti}_{\text{M2}}^{\bullet\bullet} \text{V}_{\text{Si(a)}}^{\bullet\bullet\bullet\bullet} \text{OH}_{\text{O1}}^{\bullet} \text{OH}_{\text{O3}}^{\bullet}\}$	-62973.42
$\{\text{Ti}_{\text{M2}}^{\bullet\bullet} \text{V}_{\text{Si(a)}}^{\bullet\bullet\bullet\bullet} \text{OH}_{\text{O2}}^{\bullet} \text{OH}_{\text{O3}}^{\bullet}\}$	-62973.43
$\{\text{Ti}_{\text{M2}}^{\bullet\bullet} \text{V}_{\text{Si(a)}}^{\bullet\bullet\bullet\bullet} \text{OH}_{\text{O3}}^{\bullet} \text{OH}_{\text{O3}}^{\bullet}\}$	-62973.66
$\{\text{Ti}_{\text{M2}}^{\bullet\bullet} \text{V}_{\text{Si(b)}}^{\bullet\bullet\bullet\bullet} \text{OH}_{\text{O1}}^{\bullet} \text{OH}_{\text{O2}}^{\bullet}\}$	-62973.29
$\{\text{Ti}_{\text{M2}}^{\bullet\bullet} \text{V}_{\text{Si(b)}}^{\bullet\bullet\bullet\bullet} \text{OH}_{\text{O1}}^{\bullet} \text{OH}_{\text{O3(a)}}^{\bullet}\}$	-62973.29
$\{\text{Ti}_{\text{M2}}^{\bullet\bullet} \text{V}_{\text{Si(b)}}^{\bullet\bullet\bullet\bullet} \text{OH}_{\text{O1}}^{\bullet} \text{OH}_{\text{O3(b)}}^{\bullet}\}$	-62973.51
$\{\text{Ti}_{\text{M2}}^{\bullet\bullet} \text{V}_{\text{Si(b)}}^{\bullet\bullet\bullet\bullet} \text{OH}_{\text{O2}}^{\bullet} \text{OH}_{\text{O3(a)}}^{\bullet}\}$	-62971.26
$\{\text{Ti}_{\text{M2}}^{\bullet\bullet} \text{V}_{\text{Si(b)}}^{\bullet\bullet\bullet\bullet} \text{OH}_{\text{O2}}^{\bullet} \text{OH}_{\text{O3(b)}}^{\bullet}\}$	-62973.46
$\{\text{Ti}_{\text{M2}}^{\bullet\bullet} \text{V}_{\text{Si(b)}}^{\bullet\bullet\bullet\bullet} \text{OH}_{\text{O3(a)}}^{\bullet} \text{OH}_{\text{O3(b)}}^{\bullet}\}$	-62973.46
$\{\text{Ti}_{\text{M2}}^{\bullet\bullet} \text{V}_{\text{Si(c)}}^{\bullet\bullet\bullet\bullet} \text{OH}_{\text{O1}}^{\bullet} \text{OH}_{\text{O2}}^{\bullet}\}$	-62972.82
$\{\text{Ti}_{\text{M2}}^{\bullet\bullet} \text{V}_{\text{Si(c)}}^{\bullet\bullet\bullet\bullet} \text{OH}_{\text{O1}}^{\bullet} \text{OH}_{\text{O3}}^{\bullet}\}$	-62972.82
$\{\text{Ti}_{\text{M2}}^{\bullet\bullet} \text{V}_{\text{Si(c)}}^{\bullet\bullet\bullet\bullet} \text{OH}_{\text{O2}}^{\bullet} \text{OH}_{\text{O3}}^{\bullet}\}$	-62973.05
$\{\text{Ti}_{\text{M2}}^{\bullet\bullet} \text{V}_{\text{Si(c)}}^{\bullet\bullet\bullet\bullet} \text{OH}_{\text{O3}}^{\bullet} \text{OH}_{\text{O3}}^{\bullet}\}$	-62973.05
$\{\text{Ti}_{\text{M2}}^{\bullet\bullet} \text{V}_{\text{Si(d)}}^{\bullet\bullet\bullet\bullet} \text{OH}_{\text{O1}}^{\bullet} \text{OH}_{\text{O2}}^{\bullet}\}$	-62974.18
$\{\text{Ti}_{\text{M2}}^{\bullet\bullet} \text{V}_{\text{Si(d)}}^{\bullet\bullet\bullet\bullet} \text{OH}_{\text{O1}}^{\bullet} \text{OH}_{\text{O3}}^{\bullet}\}$	-62973.43
$\{\text{Ti}_{\text{M2}}^{\bullet\bullet} \text{V}_{\text{Si(d)}}^{\bullet\bullet\bullet\bullet} \text{OH}_{\text{O2}}^{\bullet} \text{OH}_{\text{O3}}^{\bullet}\}$	-62973.42
$\{\text{Ti}_{\text{M2}}^{\bullet\bullet} \text{V}_{\text{Si(d)}}^{\bullet\bullet\bullet\bullet} \text{OH}_{\text{O3}}^{\bullet} \text{OH}_{\text{O3}}^{\bullet}\}$	-62972.07
$\{\text{Ti}_{\text{M1}}^{\bullet\bullet} \text{V}_{\text{Si(a)}}^{\bullet\bullet\bullet\bullet} \text{OH}_{\text{O1}}^{\bullet} \text{OH}_{\text{O2}}^{\bullet}\}$	-62973.35
$\{\text{Ti}_{\text{M1}}^{\bullet\bullet} \text{V}_{\text{Si(a)}}^{\bullet\bullet\bullet\bullet} \text{OH}_{\text{O1}}^{\bullet} \text{OH}_{\text{O3(a)}}^{\bullet}\}$	-62974.63
$\{\text{Ti}_{\text{M1}}^{\bullet\bullet} \text{V}_{\text{Si(a)}}^{\bullet\bullet\bullet\bullet} \text{OH}_{\text{O1}}^{\bullet} \text{OH}_{\text{O3(b)}}^{\bullet}\}$	-62974.63
$\{\text{Ti}_{\text{M1}}^{\bullet\bullet} \text{V}_{\text{Si(a)}}^{\bullet\bullet\bullet\bullet} \text{OH}_{\text{O2}}^{\bullet} \text{OH}_{\text{O3(a)}}^{\bullet}\}$	-62973.49
$\{\text{Ti}_{\text{M1}}^{\bullet\bullet} \text{V}_{\text{Si(a)}}^{\bullet\bullet\bullet\bullet} \text{OH}_{\text{O2}}^{\bullet} \text{OH}_{\text{O3(b)}}^{\bullet}\}$	-62974.63 (*)
$\{\text{Ti}_{\text{M1}}^{\bullet\bullet} \text{V}_{\text{Si(a)}}^{\bullet\bullet\bullet\bullet} \text{OH}_{\text{O3(a)}}^{\bullet} \text{OH}_{\text{O3(b)}}^{\bullet}\}$	-62974.63
$\{\text{Ti}_{\text{M1}}^{\bullet\bullet} \text{V}_{\text{Si(b)}}^{\bullet\bullet\bullet\bullet} \text{OH}_{\text{O1}}^{\bullet} \text{OH}_{\text{O2}}^{\bullet}\}$	-62972.67
$\{\text{Ti}_{\text{M1}}^{\bullet\bullet} \text{V}_{\text{Si(b)}}^{\bullet\bullet\bullet\bullet} \text{OH}_{\text{O1}}^{\bullet} \text{OH}_{\text{O3(a)}}^{\bullet}\}$	-62972.66
$\{\text{Ti}_{\text{M1}}^{\bullet\bullet} \text{V}_{\text{Si(b)}}^{\bullet\bullet\bullet\bullet} \text{OH}_{\text{O1}}^{\bullet} \text{OH}_{\text{O3(b)}}^{\bullet}\}$	-62972.68
$\{\text{Ti}_{\text{M1}}^{\bullet\bullet} \text{V}_{\text{Si(b)}}^{\bullet\bullet\bullet\bullet} \text{OH}_{\text{O2}}^{\bullet} \text{OH}_{\text{O3(a)}}^{\bullet}\}$	-62972.68
$\{\text{Ti}_{\text{M1}}^{\bullet\bullet} \text{V}_{\text{Si(b)}}^{\bullet\bullet\bullet\bullet} \text{OH}_{\text{O2}}^{\bullet} \text{OH}_{\text{O3(b)}}^{\bullet}\}$	-62972.69
$\{\text{Ti}_{\text{M1}}^{\bullet\bullet} \text{V}_{\text{Si(b)}}^{\bullet\bullet\bullet\bullet} \text{OH}_{\text{O3(a)}}^{\bullet} \text{OH}_{\text{O3(b)}}^{\bullet}\}$	-62972.89
$\{\text{Ti}_{\text{Si(a)}}^{\times} \text{V}_{\text{M1}}^{\bullet\bullet} \text{OH}_{\text{O2(a)}}^{\bullet} \text{OH}_{\text{O2(b)}}^{\bullet}\}$	-62973.17
$\{\text{Ti}_{\text{Si(b)}}^{\times} \text{V}_{\text{M1}}^{\bullet\bullet} \text{OH}_{\text{O2(a)}}^{\bullet} \text{OH}_{\text{O2(b)}}^{\bullet}\}$	-62973.28 (*)